INSTITUT DE FRANCE
Académie des sciences

Comptes Rendus
Physique

Matthieu Micoulaut

Topological ordering during flexible to rigid transitions in disordered networks

Volume 24, Special Issue S1 (2023), p. 133-154

Online since: 20 April 2023
Issue date: 26 April 2024

Part of Special Issue: From everyday glass to disordered solids
Guest editors: Jean-Louis Barrat (Université Grenoble-Alpes, France) and Daniel Neuville (Université de Paris, Institut de physique du globe de Paris, CNRS, France)

https://doi.org/10.5802/crphys.128

The Comptes Rendus. Physique *are a member of the Mersenne Center for open scientific publishing*
www.centre-mersenne.org — e-ISSN : 1878-1535

Comptes Rendus
Physique
2023, Vol. 24, Special Issue S1, p. 133-154
https://doi.org/10.5802/crphys.128

From everyday glass to disordered solids / *Du verre quotidien aux solides désordonnés*

Topological ordering during flexible to rigid transitions in disordered networks

Ordonnancement topologique lors des transitions flexible-rigide dans les réseaux désordonnés

Matthieu Micoulaut [a]

[a] Sorbonne Université, Physique théorique de la matière condensée, CNRS UMR 7600, 4 place Jussieu 75252 Paris cedex 05 France

E-mail: matthieu.micoulaut@sorbonne-universite.fr (M. Micoulaut)

Abstract. This contribution focuses on the structural origin of flexible to rigid transitions and the possible underlying intermediate phase which have been reported to occur in a variety of network glasses such as chalcogenides or modified oxides. Here, using molecular dynamics simulations of densified glass-forming liquids, $2SiO_2$-Na_2O, which are known to display a numerical reversibility window as a signature of an intermediate phase, we focus on structural functions emphasizing topological ordering using the Bhatia–Thornton formalism. Results not only reveal that densified silicates display topological ordering on lengthscales of about 25 Å, but also display obvious threshold behaviors close to the isostatic condition when the network undergoes a flexible to rigid transition. The mechanical constraint count of the atomic network structure reveals that a typical lengthscale characterizing the decay of topological correlations emerges for stressed rigid systems at ≃3.5 Å, whereas small wavevector oscillations are found to be minimal when the isostatic condition is merely satisfied. An additional analysis building on diffusivity and liquid entropy suggests that the *locus* of flexible to rigid transitions has also connections with water-like anomalies of densified tetrahedral liquids.

Résumé. Cette contribution se concentre sur l'origine structurale des transitions de flexible à rigide et une possible phase topologique intermédiaire sous-jacente qui se produisent dans une variété de verres structuraux tels que les chalcogénures ou les oxydes modifiés. Ici, en utilisant des simulations de dynamique moléculaire de liquides vitreux densifiés, $2SiO_2$-Na_2O, qui sont connus pour présenter une fenêtre de réversibilité en pression lors d'une transition vitreuse numérique, nous nous concentrons sur des corrélations structurales mettant l'accent sur l'ordre topologique en utilisant le formalisme de Bhatia–Thornton. Les résultats révèlent non seulement que les silicates densifiés présentent un ordre topologique sur des échelles de longueur d'environ 25 Å, mais présentent également des comportements de seuil évidents à proximité de la condition isostatique lorsque le réseau subit une transition de flexible à rigide. Le comptage des contraintes mécaniques de la structure du réseau atomique révèle qu'une échelle de longueur typique caractérisant la décroissance des corrélations topologiques émerge pour les systèmes rigides sous-contraints à ≃3,5 Å, alors que les petites oscillations du vecteur d'onde sont minimales lorsque la condition isostatique est simplement satisfaite. Une analyse supplémentaire basée sur la diffusivité et l'entropie du liquide suggère que le lieu des transitions de flexible à rigide a également des liens avec les anomalies observés dans les liquides tétraédriques densifiés comme l'eau sous pression.

Keywords. Glasses, structure, network rigidity, elastic phase transitions, molecular dynamics simulations.

Mots-clés. verres, structure, rigidité du réseau, transitions de phase élastiques, simulations de dynamique moléculaire.

Funding. The author acknowlegdes base and recurrent funding from Sorbonne Université and CNRS. He no longer wishes to be supported by research grants from the controversial Agence nationale de la recherche (ANR).

Manuscript received 14 June 2022, revised 14 October 2022, accepted 19 October 2022.

1. Introduction : from mean-field rigidity to reversibility windows

The atomic scale description of non-crystalline solids and glasses has remained a challenging field of inquiry in materials science because of the lack of translational periodicity that prevents from using powerful techniques offered by e.g. crystalline band theory such as Brillouin zones, k-space and Bloch functions. In addition, the structural information gathered from light, neutron or X-ray scattering often remains at the level of short order (bond distances, coordination numbers) as long-range order made of the repetition of a well-defined unit cell is notoriously absent. Some information can be gathered from the low wave-vector region of e.g. the structure factor and permits to correlate salient features of scattering functions such as the first sharp diffraction peak (FSDP) to certain features of atomic ordering [1–3]. Only a limited number of glasses where structural groupings are present, essentially ring structures, can be unambiguously analysed and their structure characterized from explicit spectroscopic signatures using Raman or Nuclear Magnetic Resonance (NMR) spectroscopy [4–6]. On the theoretical side, atomistic simulations can be extremely valuable for understanding structural and dynamic properties including aspects of the glass transition and relaxation of the supercooled state [7]. They also appear to be useful for checking the validity of microscopic models, empirical approximations or theoretical assumptions. The present contribution clearly belongs to this general scope, and attempts to link certain features derived from simulations with results from rigidity theory.

The concept of rigidity in amorphous networks and glasses traces back to the early work of Maxwell on the stability of macroscopic structures such as bridges or roof frameworks [8], and to the introduction of mechanical constraints by Lagrange. These ideas and results were then extended to atomic networks by Phillips [9] who highlighted the notion of mechanical isostaticity as promoting glass-forming tendency of covalent alloys. It was recognized that so-called "good" glass formers usually form at an optimal network connectivity, or mean coordination number satisfying the Maxwell stability criterion of isostatic structures, i.e. $n_c = 3$ in 3D, where n_c is the count of atomic constraints per atom arising from relevant neighbor interactions.

1.1. *Mean-field molecular rigidity*

It is useful to review basic results from the Phillips–Thorpe mean-field rigidity theory [10]. In structural glasses the relevant interactions can be near-neighbor bond-stretching (BS) and next-near-neighbor bond-bending (BB) forces that characterize bonds and angles typical of the network topology. In a mean-field approach, the atomic density n_c of mechanical constraints can be exactly computed, and is given by:

$$n_c = \frac{\sum\limits_{r\geq 2} n_r \left[\frac{r}{2} + 2r - 3\right]}{\sum\limits_{r\geq 2} n_r} \tag{1}$$

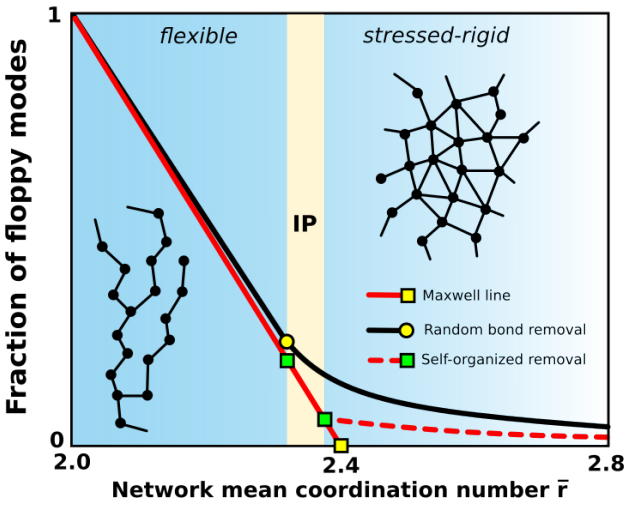

Figure 1. Fraction of floppy modes { as a function of average network coordination number $\bar{r}$ (adapted from Ref. [15]). The mean-field Maxwell line $f = 3 - n_c = 6 - 5\bar{r}/2$ vanishes exactly at $\bar{r}$=2.4 (solid red curve, eq. (3)), whereas percolation of rigidity is obtained from bond-depleted networks at a somewhat lower connectivity (solid black, [10]). At T=0, a self-organized removal of bonds (avoiding the presence of stressed rigidity, solid and broken red curve) leads to two percolative stress and rigidity transitions (green squares), and define a so-called intermediate phase (IP). See also Figure 2.

where n_r is the concentration of species being r-fold coordinated. Here it should be noted that the temperature is absent. The contribution of the two terms in the numerator is straightforward because each bond is shared by two neighbors, and one has therefore $r/2$ bond-stretching (BS) constraints for a r-fold atom. For BB (angular) constraints, one notices that a 2-fold atom involves only one angle, and each additional bond needs the definition of two more angles, leading to the estimate of ($2r$-3). For one-fold terminal atoms, a special count [11] is achieved as no BB constraints are involved, and in certain situations some constraints may be ineffective [12, 13]. By defining the network mean coordination number $\bar{r}$ of the network by:

$$\bar{r} = \frac{\sum\limits_{r\geq 2} r n_r}{\sum\limits_{r\geq 2} n_r} \tag{2}$$

one can reduce (1) to the simple equation:

$$n_c = \frac{\bar{r}}{2} + 2\bar{r} - 3 \tag{3}$$

It is easy to verify that the Maxwell isostatic criterion (n_c=3) corresponds to a threshold average coordination number [9, 10] of $\bar{r}$=2.40 in 3D, corresponding usually to a non-stoichiometric composition where glass-forming tendency has been found to be optimized experimentally (e.g. $GeSe_4$ instead of the silica analog $GeSe_2$ in the Ge-Se system), including in systems with a strong crystallization tendency [14].

The nature of the underlying phase transition associated with the isostatic criterion has been revealed from a vibrational analysis of bond-depleted random networks [10, 16] constrained by harmonic bond-bending and bond-stretching interactions. In such networks, the number of zero frequency (floppy) modes $f = 3\text{-}n_c$ (i.e. the eigenmodes of the dynamical matrix) is vanishing for $\bar{r}$=2.38 when rigidity percolates through the network (Figure 1). The Maxwell condition $n_c = 3$

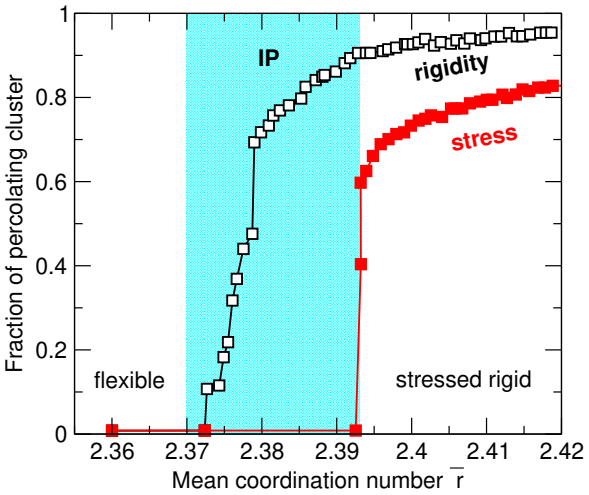

Figure 2. Evidence for a stress-free intermediate phase (IP) from the Pebble Game analysis (adapted from [15,27]). Fraction of sites on isostatically rigid and stressed rigid percolating cluster in a self-organized network as a function of the network mean coordination number $\bar{r}$. The intermediate phase which is rigid but unstressed exists in these classes of models between $\bar{r}_{c1}$=2.375≤ $\bar{r}$ ≤ 2.392=$\bar{r}_{c2}$, and coalesces in random networks.

therefore defines a mechanical stiffness transition above which redundant constraints produce internally stressed networks, identified with a stressed-rigid phase [16]. Here, $\bar{r}$ acts as the external control parameter of the transition, whereas f is the order parameter. For n_c <3 however, floppy modes can proliferate, and these lead to a flexible phase where local deformations with a low cost in energy (typically 5 meV [17]) are possible, their density being given by: $f = 3 - n_c$. There have been early experimental probes of this peculiar transition from Raman scattering [18], stress relaxation [19] and viscosity measurements [20–22], vibrational density of states [17], Brillouin scattering [13,23], resistivity [24,25], and Kohlrausch exponents [19,26].

1.2. *Beyond mean-field*

The construction leading to the mean-field constraint estimate (eq. (3)) neglects fluctuations that have been identified numerically at finite temperature [28,29] and considers only network averaged quantities, i.e. one assumes that all atoms of a given type have the same constraint density arising from an identical coordination number per chemical species. However, as in ordinary phase transitions fluctuations in constraints or in the order parameter f may be expected close to the critical point at n_c = 3. It has been suggested (for a review, see [30]) that this non-mean field scenario manifests by the onset of an isostatic or intermediate phase (IP) in which fluctuations in coordination may be important, as well as network adaptation in order to lower the stress induced by the increasing cross-link density during the glass transition (red curves, Figure 1).

A certain number of scenarios have been proposed to describe the observed behaviors, and these emphasize either the role of fluctuations in the existence of a double threshold/transition defining an IP between the flexible and the stressed rigid phase [15, 31–34], or on a non-trivial elastic coupling between atoms with limited coordination fluctuations [27, 35]. In the latter scenarios, such approaches lead to the emergence of locally distinct configurations that promote an IP.

Following the path based on coordination fluctuations, several authors have modified the initial mean-field theory [9, 10] to account for structural adaptation or self-organization in order to avoid stress from additional cross-linking elements with an energy penalty if stressed rigid elements are considered [15,31,32,34,36]. This adaptation has been also revealed from molecular simulations showing that rigid angles will soften (adapt) with increasing stress/pressure in order to reduce the global increase of the constraint density upon cooling the melt [37]. In spirit, these models (built from lattices [15,36], clusters [32,33], spin cavity expansions [31]), share in common that the addition of bonds in a network with increasing average connectivity will be accepted only if this leads to isostatically rigid regions. Once the network has undergone percolation of rigidity at a first transition at $\bar{r}_{c1}$, an unstressed (isostatic) structure dominates, and characterizes the IP. The addition of redundant bonds then will contribute to the occurrence of stressed rigid regions clusters that finally percolate at a second transition at $\bar{r}_{c2}$, identified with a stress transition. Both transitions then define a window in connectivity $\Delta\bar{r}=\bar{r}_{c2}-\bar{r}_{c1}$ (Figure 2).

Instead, using models of soft spheres in the context of jamming transitions, different authors [27, 35] have suggested that the IP could result from the presence/absence of weak non-covalent interactions in addition to harmonic elastic interactions. In a strong force régime, an IP can be obtained that is characterized by an isostatic cluster spanning the whole system, driven by fluctuations in coordination. However, when weak interactions are present, these features vanish below a certain temperature suggesting that the transitions become mean-field at low temperature and coalesce. These results are partially supported by MD simulations [37] taking into account long-range interactions (Coulomb, Van der Waals) allowing to probe the weak-force régime.

1.3. *Reversibility windows*

Experimental support to the predictions of non-mean-field rigidity is obtained from various probes (Figure 3), the main one being of calorimetric nature. Modulated differential scanning calorimetry at the glass transition permits, indeed, to measure an enthalpy of relaxation (a non-reversing heat flow ΔH_{nr}) which exhibits a deep minimum over a finite compositional interval, sometimes exhibiting even sharp boundaries and a square-well behavior with composition defining a reversibility window (RW) for which $\Delta H_{nr} \simeq 0$. The latter behavior is thought to be a $T \neq 0$ manifestation of the intermediate phase characterizing the $T = 0$ disordered network representing the model glass [30]. There is actually a strong experimental support for these findings connecting RW with the isostatic nature of the network glass structure, and a vast literature has been accumulated on this topic during the last decade for a variety of systems, modified oxides or chalcogenides, which exhibit a salient phenomenology of thermal, relaxation, and vibrational anomalies (Figure 3). A certain number of measured anomalies are provided for Ge-Se (Figure 3a) [39] and AgI-$AgPO_3$ (Figure 3b) [26]. The former indicates that for isostatic compositions, a near stress-free character is suggested from Raman pressure experiments [38] and manifests by a zero threshold pressure in the IP, as in crystals without residual stresses. Corresponding volumes are found to be minimum and indicate space-filling tendencies (Figure 3a, right axis [39]). In a very different glass (AgI-$AgPO_3$), the boundaries of the RW [24] coincide with a marked jump in ionic conductivity that grows exponentially once the network has become flexible (Figure 3b, right axis [26]). It indicates that local deformation (floppy) modes will promote ion hopping. These changes are accompanied by a maximum in dielectric permittivity (left axis). Glasses with various bonding types display RWs (Figure 4), from ionic (silicates [13]) to iono-covalent, covalent (Ge-Se, [21]), or semi-metallic (Ge-Te-In-Ag [41]). In certain of these systems, e.g. for the simple binary network glasses such as Ge_xS_{1-x} or Si_xSe_{1-x}, the experimental boundaries of the RW are found to be all very close [21, 42, 43], i.e. located between 20 % $< x <$ 25 %, and aspects of

topology fully control the evolution of rigidity with composition, given that there is a weak chemical effect in case of isovalent Ge/Si or S/Se substitution. This compositional interval defining the RW connects to the mean-field estimate of the isostatic criterion (eq. (3)) satisfying $n_c = 3$ because coordination numbers of Ge/Si and S/Se can be determined from the 8-$\mathcal{N}$ (octet) rule to yield an estimate of the constraints n_c=2+5x using eq. (1). In fact, for these IV-VI glasses, the lower boundary of the RW (x_c=20 %) coincides with the Phillips–Thorpe [9,10] mean-field rigidity transition n_c=3 and $\bar{r}$=2.4.

For most of the systems however, a direct constraint counting cannot be performed because uncertainties persist regarding the relevant coordination numbers so that an enumeration of active/inactive constraints must be derived from specific structural models (see, e.g. an example for silicates [13]). This feature becomes obvious once Group V selenides/sulphides are being considered (Figure 4). Here, different RW locations are found for isovalent compounds, e.g. differences emerge between As- and P-bearing chalcogenides, and between sulphides and selenides (e.g.

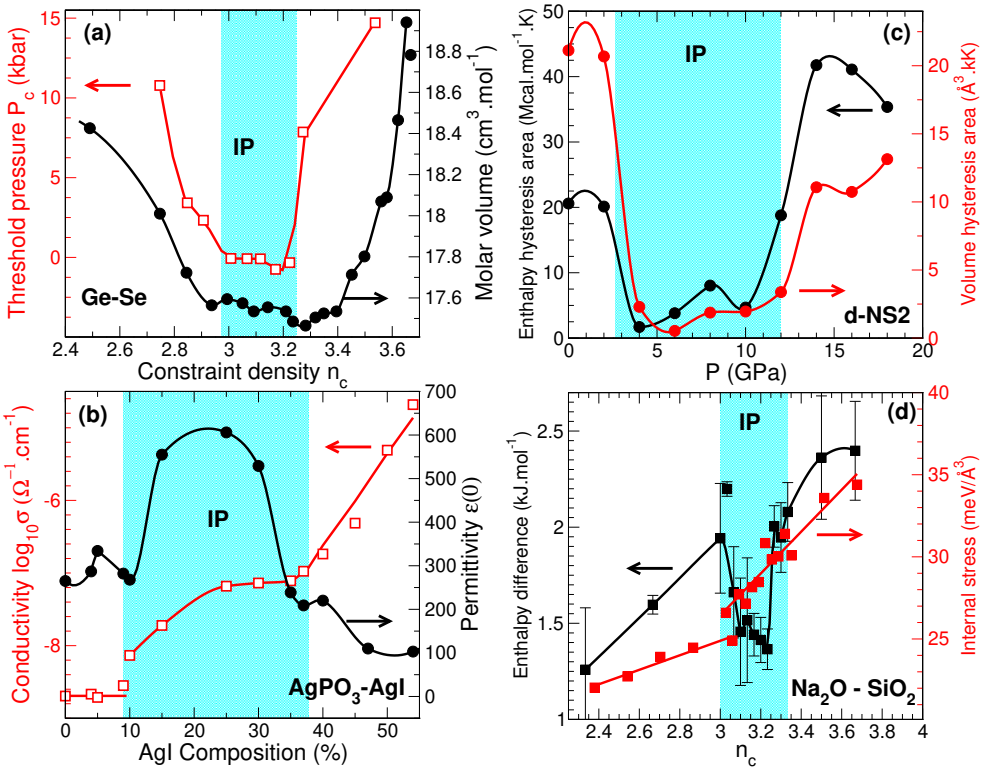

Figure 3. Experimental and numerical verification of anomalies in the intermediate phase region (cyan background) for different glassy systems : (a) Raman threshold pressure (red) and molar volume (right axis) as a function of constraint density in Ge-Se glasses [38, 39]. (b) Ionic conduction (red) and dielectric permittivity $\varepsilon(0)$ (right axis) as a function of AgI content x in (1-x)$AgPO_3$-xAgI glasses [24, 26]. (c) Calculated enthalpy and volume hysteresis (red, right axis) as a function of pressure in MD simulations of densified silicates [37]. (d) Calculated enthalpy and internal network stress (red right axis) as a function of the calculated constraint density in (1-x)Na_2O-$xSiO_2$ [40]. The cyan areas represent the reversibility window determined experimentally [39] or numerically [37, 40] in the glass transition region.

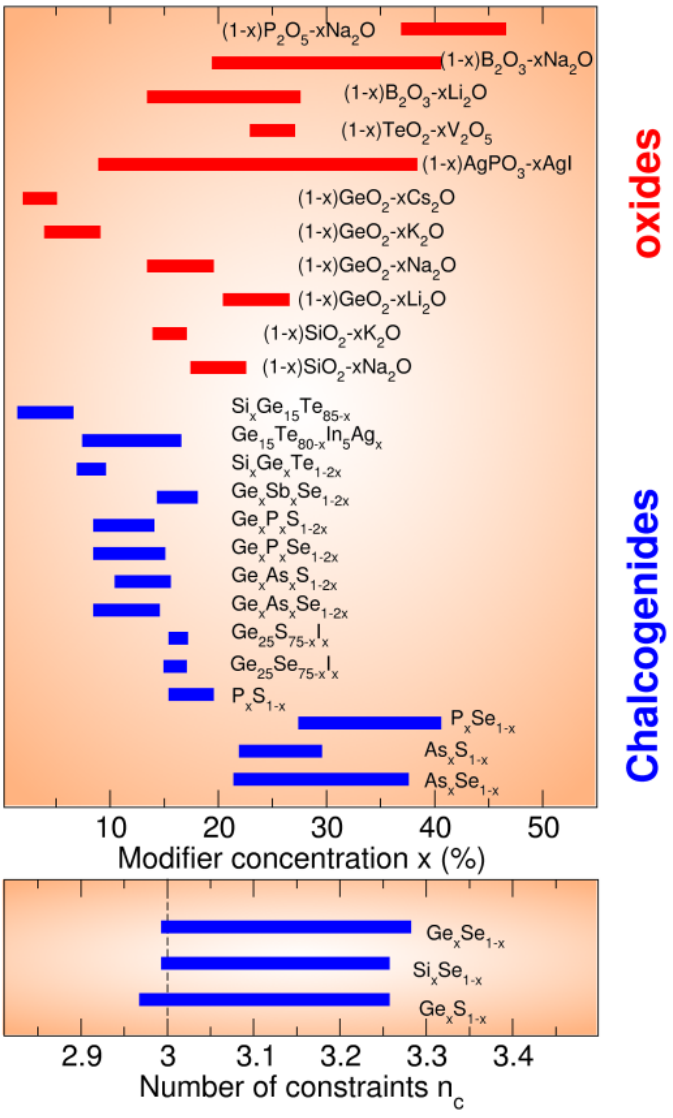

Figure 4. Experimental location of reversibility windows thought to be the manifestation of the topological intermediate phase predicted from models : modified oxides (phosphates [24, 44], borates [6], germanates [45], silicates [13]) and chalcogenides (Si-Ge-Te [46, 47], Ge-Te-In-Ag [41], Ge-Sb-Se [48], Ge-P-S [49], Ge-P-Se [50], Ge-As-S [51], Ge-As-Se [52], Ge-S-I [53], Ge-Se-I [54], P-S [55], P-Se [56], As-S [57], As-Se [22]). Only a limited cases can be represented as a function of constraint density given the obvious atomic coordinations fulfilling the octet rule : Ge-S [43], Ge-Se [39], and Si-Se [42].

P_xS_{1-x} and P_xSe_{1-x}, [49]) so that differences can only be explained from structural models validated from e.g. spectroscopic studies [56]. The above statements are also valid in tellurides for which the increased electronic delocalization of the Te atoms lead to mixed local geometries that are now composition dependent [14], so that a proper constraint count must rely on molecular simulations, in conjunction with dedicated constraint counting algorithms.

Molecular dynamics simulations have been able to substantiate the characteristics of RWs [37, 40, 58, 59]. Using a similar methodology as the one used in experimental calorimetry, cooling-heating cycles have been performed in pressurized silicates (Figure 3c [37]) and sodium silicates ((Figure 3d). Concerning the latter, the hysteresis resulting from enthalpic relaxation during a numerical cooling-heating cycle has been found to be minimized for 12 %$\leq x \leq$ 20% Na_2O (Figure 3d [40]), which echoes with the experimental observation of the RW (18 %$\leq x \leq$ 22% Na_2O [23]). For both investigated silicates, the location of the RW corresponds to an isostatic character of the network that is independently computed. In addition, a certain number of other anomalies have been found from simulations, such as minimal activation energies in viscosity and diffusivity [60], minimal relaxation time [37], growth of internal stress (Figure 3d, right axis [40]) with a marked jump at the stress transition.

1.4. *The structural signature of the intermediate phase*

In the present work, we examine structural features that could be associated with the onset of stressed rigidity or the IP. The question continues to be actively debated in the literature given the rather elusive structural signatures of rigidity transitions in spite of thermal and spectroscopic evidence. Direct structural signatures have been searched by different authors. For instance, X-ray diffraction in Ge-Se glasses [61, 62] have revealed that the area and the inverse position of the first sharp diffraction peak of the structure factor $S(k)$ exhibited a plateau found in the same compositional window as the reported IP, i.e. suggesting some effect of intermediate range order for isostatic compositions. These conclusions were not confirmed by a similar study [63] and the reported x-ray absorption fine structure analysis furthermore found no correlation between the short-range order and the IP, as also evidenced from various NMR studies [64, 65]. Another x-ray absorption experiment on Ge-Se (near-edge structure) on Ge-Se glasses led to an opposite conclusion [66] as spectra revealed compositional plateaus coinciding with the location of the RW, providing structural evidence for the IP. More recently, the possibility of a structural signature of the IP in Ge-Se has been examined from high-resolution neutron diffraction to measure different quantities associated with topology [67], and results did not point to an obvious structural origin of the IP. For instance, they did not confirmed the possible deviation of atomic coordinations from the 8-N rule reported from first-principles molecular dynamics simulations [68].

Molecular simulations have, indeed, attempted to characterize the origin of the IP. On the archetypal Ge-Se system, first principles simulations have shown that isostatic glasses originate from a competition between amorphous $GeSe_2$ and amorphous Se clusters to produce measurable signatures in electronic properties [66, 68]. On the same system, it was shown that while no compelling evidence for signatures were found in structure functions (pair correlation $g(r)$, structure factor $S(k)$, in contrast with simulated As-Se glasses [69, 70]), constraint-counting algorithms showed that broken bond-bending constraints are associated with the stressed-rigid phase, a result that was also recovered for As-Se [70] and Ge-S glasses [71]. The softening of bending constraints under increased applied stress *via* cross-linking or applied pressure turns out to be a specific feature in stressed rigid systems and this feature has been also found in different densified tetrahedral liquids [72, 73].

The most noticeable structural anomaly related with onset of rigidity has been determined for selected systems only. While principal peak characteristics (position, width) of total scattering functions do not display any specific trend related to the underlying phases [1, 67], partial correlations in Fourier space reveal that some change in structural ordering takes place as networks become rigid. This is exemplified in densified $2SiO_2$-Na_2O for which the FSDP found at ambient pressure (at wavevector position k_{FSDP}=1.53 Å^{-1}) evolves monotonically up to 1.9 Å^{-1} with

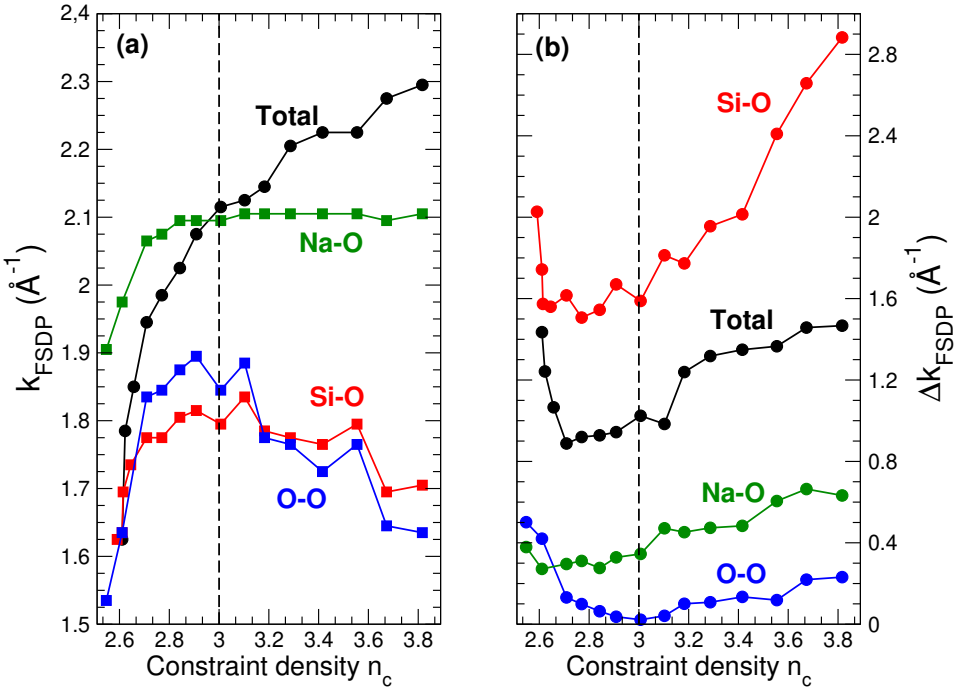

Figure 5. (a) Position k_{FSDP} of the FSDP (in Å^{-1}) of different partial structure factors as a function of the calculated constraint density n_c. (b) Width Δk_{FSDP} of the FSDP (in Å^{-1}). Adapted from Ref. [60]

pressure/rigidity (black curve, Figure 5a). The behavior contrasts with the one calculated for corresponding network partials (Si-O, O-O [60]) which peak at $n_c \simeq 3$. Corresponding trends are obtained for the width of the FSDP (Figure 5b). As the position of the FSDP reflects some repetitive characteristic distance between structural units, the result indicate that an intermediate range order lengthscale of distance $7.7/k_{FSDP}$ emerges, and then decreases. Here the factor 7.7 relates to the first maximum of the spherical Bessel function $j_0(kr)$. Similarly, the broadening of the FSDP is indicative of a correlation length, following the well-known Scherrer equation for microcrystals which connects the width Δk_{FSDP} of a Bragg peak with the average size of the microcrystals. Similar features have been obtained for partials in the As-Se system [69, 70]. While, the total structure factor characteristics did not showed any specific trend across the rigidity transitions as in experiment [1], it was found that k_{FSDP} of the As-Se partial structure factor displayed a threshold behavior at the Se-rich boundary of the IP, whereas Δk_{FSDP} displayed a minimum value in the IP. These findings indicate that structural features might be material specific, and the question of structural correlations in relationship with flexible to rigid transitions continues to be questioned.

Here, inspired by the work of Wilson [74] and using large scale molecular dynamics we are able to probe such structural correlations up to 20-25 Å in a network (sodium silicate) that is known [37] to undergo flexible-intermediate-stress transitions/thresholds, to display a RW (Figure 3c) and a series of anomalies in dynamic heterogeneities [28, 29]. By focusing on structure functions describing topological ordering at long-range (Bhatia–Thornton formalism), we show that a typical lengthscale of about 3.5 Å characterizing the decay of correlations emerges once the system becomes rigid. Similarly, the wavevector characterizing the long-range oscillations of topological ordering is found to be minimal for a calculated $n_c \simeq 3$ which signals that peri-

odic ordering takes place on larger lengthscales in isostatic networks. Since we are focusing on structural correlations, we also calculate the pair correlation entropy which measures excess contributions with respect to a non-structured reference state, and maximizes for $n_c \simeq 3$. Taken together, these results indicate that isostatic systems bear striking similarities with densified tetrahedral liquids displaying water-like anomalies, i.e. correlated extrema in transport coefficient (diffusivity), thermodynamics, excess entropy and structural features. These commonalities are discussed and contrasted.

2. Simulation methods

2.1. *System characteristics*

The system under investigation is a densified sodium silicate supercooled liquid ($2SiO_2$-Na_2O, or NS2) that has been investigated from classical MD simulations (integration time using the Verlet algorithm with a 1 fs time step). The atoms interact with a rigid ion two-body potential parametrized by Teter [75] of the form :

$$\Phi_{ij}(r) = \Phi_{ij}^{SR}(r) - \frac{C_{ij}}{r^6} + \frac{q_i q_j}{r} \tag{4}$$

where $\Phi_{ij}^{SR}(r) = A_{ij} \exp -\rho_{ij}/r$ is a short-range term arising from electronic repulsion between atoms. The accuracy of the potentials has been demonstrated in various studies on structural [76–79] and dynamic properties. Noteworthy is the fact that calculated diffusion and viscosity are comparable to experimental data [80] so that the efficiency is substantially improved with respect to alternative potentials [81]. The cut-off for both Buckingham and Coulomb part of the Teter potential has been set to 18 Å.

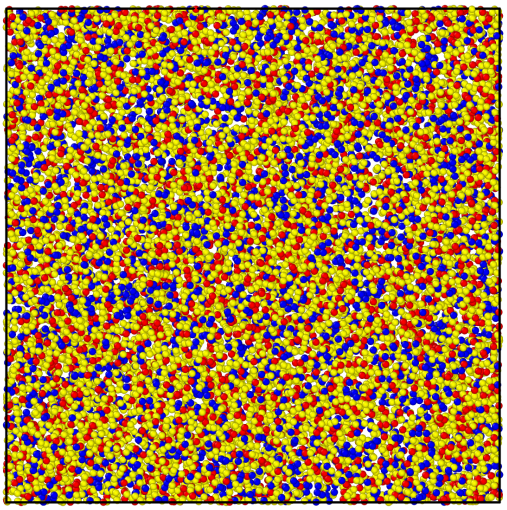

Figure 6. A snapshot of the simulated system: 16767 atoms representing the NS2 liquid (red: silicon, yellow: oxygen, blue: sodium). At zero pressure, the cell length is 65 Å.

In order to investigate long-range information of the partial pair correlations functions, the initial configuration has been obtained from a rather large crystalline disilicate sample consisting of 16767 atoms (1863 $Na_2Si_2O_5$ units). The system has been melted at an equilibration stage at 4000 K over 1 ns, prior to sequential quenches at 3500 K, 3000 K, and finally the target temperature

of 2000 K corresponding to the numerical glass transition region where the reversibility window has been obtained numerically [37]. The resulting structure (Figure 6) has a cell length at zero pressure of about L=65 Å which permits to safely consider distances up to 20 Å< $L/2$ from simulations up to the most elevated pressures. Densification has been achieved by increments up to 20.12 GPa in NPT Ensemble (L=55.39 Å).

2.2. *Molecular dynamics based rigidity*

In order to connect the structure to features of rigidity, and particularly the constraint density n_c with pressure and temperature, we enumerate mechanical constraints from the atomic scale time dependent trajectories obtained at a given thermodynamic condition (2000 K, P). Previous applications of this methodology have been performed for the particular NS2 system [37,82], but also on a variety of different chalcogenide network glasses [14,71,83] and liquids [84].

To determine the number of BS constraints, one focuses on neighbour distribution functions around a given atom i, the global sum of all such functions yielding an i-centred pair correlation function $g_i(r)$ whose integration up to the first minimum gives the coordination numbers r_i, and hence the corresponding number of BS constraints n_c^{BS}=$r_i/2$. This number usually correspond to small radial motion between two neighboring atoms.

To determine BB constraints, one uses partial bond angle distributions (PBADs) $P(\theta_{ij})$ which split the usual bond angle distribution into partial contributions defined by a central atom 0 and the N first neighbours which define N(N-1)/2 possible triplets or angles $i0j$ (i=1..N-1, j=2..N), i.e. 102, 103, 203, etc. The standard deviation σ_θ^{ij} of each distribution P(θ_{ij}) gives a quantitative estimate of the angular excursion around a mean angular value, and provides an indication of the bond-bending strength. Small values for σ_θ^{ij} correspond to an intact bond-bending constraint which maintains a rigid angle at a fixed value, whereas large σ_θ^{ij} correspond to a bond-bending weakness giving rise to an ineffective or broken constraint [82].

The use of such standard deviations permits to derive the constraint density under various thermodynamic conditions $n_c(x,T,P)$ (x-axis of Figure 3d) without any need of dedicated phenomenological structure models. Model potentials (such as eq. (4)) are validated from a successful comparison of structure functions ($g(r)$, $S(k)$) obtained from scattering experiments.

3. Results

3.1. *Bhatia–Thornton formalism and the decay of correlation functions*

In order to concentrate on long-range topological ordering, we use the Bhatia–Thornton (BT) formalism [85] which focuses on the number-number correlations (via a corresponding structure factor $g_{NN}^{BT}(r)$) whose definition for binary mixtures can be easily extended to the present ternary (Si,O,Na) system (see also Ref. [86]):

$$g_{NN}^{BT}(r) = \sum_{i,j} x_i x_j g_{ij}(r) \tag{5}$$

where $g_{ij}(r)$ represent the different calculated partial pair correlation functions (not shown). In scattering experiments, this function (or its counterpart $S_{NN}^{BT}(k)$ in Fourier space) probes correlations that are independent of the chemical nature of the scattering centers and, therefore, provides a measure on topological ordering at intermediate and extended lengthscales [2, 3] depending on position/width of the FSDP and principal peak, respectively. Other partials can be derived within this formalism and these focus on e.g. how chemical species are distributed over the scattering centers and might provide information on chemical ordering, i.e. the preference

to form unlike bonds (as Ge-Se bonds in Ge-Se glasses [2]). For a ternary alloy, concentration-concentration correlations of the silica network can e.g. be characterized via:

$$x_{Se}^{-1} g_{CC(SiO)}^{BT}(r) = x_{Si} + x_O + x_{Na}\Big[x_{Si}^2 g_{SiSi} + x_O^2 g_{OO} + 2x_{Si}x_O g_{SiO} - 2x_O(x_{Si}+x_O)g_{ONa} - 2x_{Si}(x_{Si}+x_O)g_{SiNa} + (x_{Si}+x_O)^2 g_{NaNa}\Big] \quad (6)$$

with x_{Na}=x_{Si}=0.22 and x_O=0.56 given by the stoichiometry of NS2. Note that for a three component system there are three different concentration-concentration pair correlation functions and $g_{CC(SiNa)}^{BT}(r)$ and $g_{CC(ONa)}^{BT}(r)$ are obtained by a cyclic operation on (Si,O,Na). In the high wavevector region r all concentration-concentration structure factors converge to the limit $x_i(x_j+x_k)$ ($i \neq j,k$) which is a direct consequence of the definition of $g_{CC(SiO)}^{BT}(r)$, $g_{CC(SiNa)}^{BT}(r)$ and $g_{CC(ONa)}^{BT}(r)$ (eq. (6))). We won't comment more on additional correlations (number-concentration, see Ref. [86]).

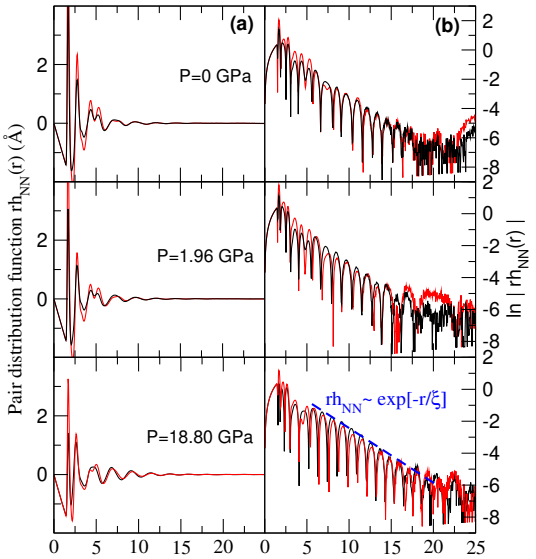

Figure 7. Plot of the Bhatia–Thornton Number-Number pair correlation function $rh_{NN}(r)$ (a) for three different pressures in NS2 : total contribution (black curve) and network contribution (SiO_2, red curve) for P=0 GPa, P=1.96 GPa and P=18.80 GPa. (b) The representation $|rh_{NN}(r)|$ [87] permits to highlight the exponential decay of the partial pair correlation function (same pressures and same color code for the contributions).

Figure 7a now represents $G_{NN}(r)$=$rh_{NN}(r)$=$r[g_{NN}(r)-1]$ for three different pressures corresponding to the flexible phase (P=0, n_c=2.92), to an isostatic condition (P=1.96 GPa, n_c=3.01) and to the stressed rigid phase (P=18.80 GPa, n_c= 3.59, see Figure 3c). Usual features of such functions are obtained and manifest by a very intense principal peak (r=1.65 Å) arising from the Si-O correlations of the base silica network, together with a secondary peak found at r=2.81 Å which is mainly due to O-O and Si-Si correlations, the alkali related correlations leading to much broader distributions with principal peaks located at 2.44 Å and 3.66 Å for Na-O and Na-Si correlations, respectively. In the region around $r \simeq$5.0 Å, the pair distribution function $rh_{NN}(r)$ is dominated by a double peak structure that is due to Si-O secondary correlations and a superposition of different partials (O-O and Si-Si), respectively. Upon increasing pressure, the principal peak shifts to larger distances (1.71 Å for 18.80 GPa) consistently with the usual tetrahedral to octahedral conversion of Si which involves a lengthening of the Si-O bonds [80]. Noteworthy is the merging of

the double peak at $r \simeq 5$ Å which is produced by a near equivalent contribution of Si-O, Na-O and Si-Si partials at high pressure.

In order to highlight the asymptotic decay of $rh_{NN}(r)$, we represent on the right side of Figure 7 the quantity $\ln|rh_{NN}(r)|$. While correlations become noisy at long-range distance due to the limited sampling of the structure at long distances ($r \geq 20$ Å), a clear signature of an exponential decay $\exp[-r/\xi]$ is acknowledged (blue curve, bottom panel in Figure 7b). This feature is present for the whole system but also if one focuses only on the underlying Si-O subnetwork red curves). The asymptotic decay of total correlation functions has been interpreted by Ma et al. [88] as the result of a self-similar packing of atomic clusters which leads to a medium range order having the characteristics of a fractal network of dimension D_f. From a variety of metallic glasses, the asymptotic decay ($r > 6$ Å) could be fitted using the functional form :

$$G(r) - 1 = Ar^{D_f - D} \exp[-r/\xi] cos\left(q_1 r + \phi\right) \tag{7}$$

with $D_f - D = D_f - 3 = 0.69$ in 3D, and ξ a cutoff length characterizing the finite cluster size and possible cluster-entanglement effects [89]. Here, the sinusoidal function $sin(q_1 r + \phi)$ was introduced to describe the oscillatory correlation of $G(r)$ with q_1 the FSDP position. A similar form inspired from the Ornstein–Zernike (OZ) theory of liquids [90] has been proposed for network glasses by Salmon and co-workers [3, 91] without invoking the need of a fractal dimension, and has been successfully applied to network glasses and liquids. The approach builds on a simple rigid-ion pair potential model of the form given in eq. (4) and an exact solution indicates that at long distance $rh_{NN}(r) \rightarrow r^{-5}$ in absence of the dispersion term (C_{ij}=0 in eq. (4)). A pole analysis [87, 92] of the k space solutions of the OZ equations then leads for the particular case of dense liquids to an exponential decay of the form:

$$G_{NN} = rh_{NN}(r) = 2A_{NN} \exp[-r/\xi] cos\left(q_1 r + \phi_{NN}\right) \tag{8}$$

with parameters ξ and q_1 that are specific to the fitted functions (h_{NN}, h_{CC} and h_{NC}) in several glasses and liquids (GeO_2, $GeSe_2$, $ZnCl_2$ [93]). Importantly, it was found that in such tetrahedral systems q_1 is not related to the FSDP position. In the present study, while dispersion terms are present in O-O, O-Si and O-Na interactions [75], the functional form proposed in eq. (8) still provides an interesting guide for examining structural correlations (see however, the effect of dispersion forces in Ref. [94]). Secondly, although the functional forms have been proposed for binary mixtures [95] and since the Bhatia–Thornton pair correlation function $rh_{NN}(r)$ also displays an obvious asymptotic decay together with an oscillatory behavior, it is tempting to use the proposed functional forms to extract an information on topological ordering with respect to the rigidity status of the considered systems.

An inspection of Figure 7b shows repeated maxima obeying a straight line $ln|rh_{NN}(r)| \simeq -r/\xi + constant$ and clearly indicates an exponential decay of the oscillations. It, therefore, represents a convenient starting point for discussing extended-range ordering, as also performed experimentally [91]. The fit using eq. (8) on the calculated functions $h_{NN}(r)$ (Figure 8) now suggests evidence that at large distance (here $r \geq 7$ Å) the damped oscillations of topological correlations can be reproduced using the OZ form. For the represented system at P=4.0 GPa, we find ξ=2.86 Å and q_1=2.61 Å^{-1}. These values already indicate that q_1 cannot be related to the FSDP position k_{FSDP} as suggested by Ma et al. [88] given our calculated k_{FSDP}=1.95 Å^{-1} [60]. Instead, q_1 is rather linked to the principal peak position found at k_{PP}=2.98 Å^{-1}, and this suggested correlation appears to hold for the experimentally investigated glasses (e.g. q_1=2.10 Å^{-1} against k_{PP}=2.04 Å^{-1} and k_{FSDP}=1.14 Å^{-1} in glassy $GeSe_2$ [3, 93]). Similarly, the obtained ξ values for the present silicates appear to be close to those obtained experimentally (e.g. ξ=3.00 Å in GeO_2 [93], represented in Figure 9b).

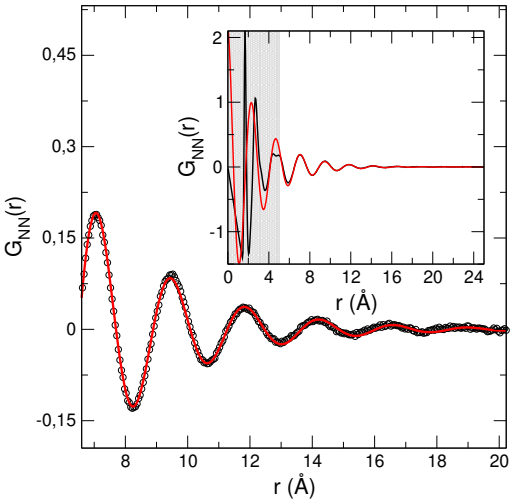

Figure 8. Calculated Bhatia–Thornton NN pair correlation function $G_{NN}(r)=r[g_{NN}(r) - 1]=rh_{NN}(r)$ for P=4.0 GPa (circles), together with a fit from eq. (8) (red curve). The inset shows the entire function with the fit, and the gray zone defines the $r-$range over which the fit has not been performed.

3.2. *Threshold behavior in topological ordering*

The resulting parameters ξ and q_1 are now represented in Figures 9 and 10 as a function of applied pressure (panels a) or calculated constraint density n_c (panels b).

When represented as a function of pressure, $\xi(P)$ leads to a smooth increase (Figure 9a), and a near constant behavior if only the SiO_2 subnetwork is considered. This typical distance converges to a limiting value of about $\simeq$3.5 Å (for the total network) that is also close to the one determined for the stressed rigid system $GeSe_2$ [93] for which a mean-field estimate leads to n_c=3.67 [30]. On the other hand, the other experimental data point (GeO_2, $n_c \simeq 3$ [96]) is compatible with the obtained trend in $\xi(n_c)$. Conversely, a minimum occurs for the parameter q_1 that characterizes the periodicity of topological ordering (Figure 10a). This minimum (less pronounced for the underlying silica network) is obtained at the flexible-intermediate boundary of the IP previously characterized [37], whereas for intermediate and stressed rigid system, a linear increase of $\xi(P)$ is acknowledged, suggesting a reduction of the periodicity of topological ordering upon further compression.

The obtained behavior obviously suggests a structural signature for the IP as also previously emphasized for peak characteristics in Fourier space at low wavevector [60]. These signatures are essentially obtained once all Faber–Ziman or BT partial correlations are being considered (Figure 5) and are, therefore, barely visible from total correlations accessed from X-ray and neutron scattering studies without isotopic substitution [63, 67]. Parameters of the FSDP region display, indeed, an anomalous behavior in some of the partial structure factors. The position k_{FSDP} maximizes for a select number of partials only (Si-O, O-O Figure 5a), whereas the width also show anomalies (minimum) close to the isostatic system.

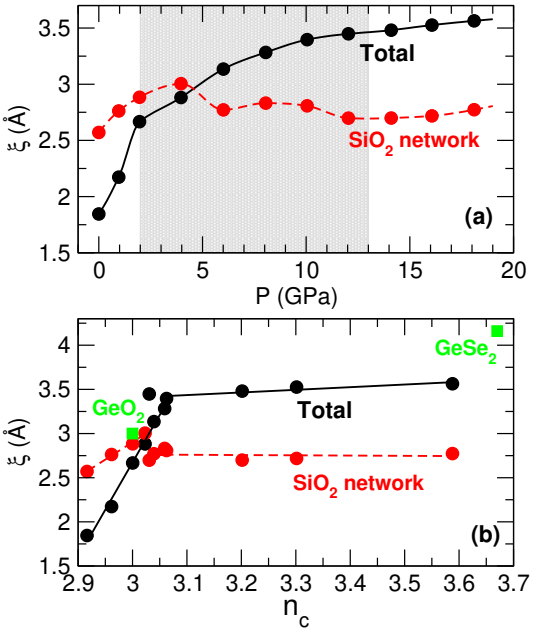

Figure 9. Distance ξ obtained from the fit of the Bhatia–Thornton pair correlation function $rh_{NN}(r)$ (Figure 8): (a) $\xi(P)$, (b) $\xi(n_c)$. The gray zone represents the reported numerical reversibility window [37]. Green symbols represent experimental data for GeO_2 and $GeSe_2$ [93].

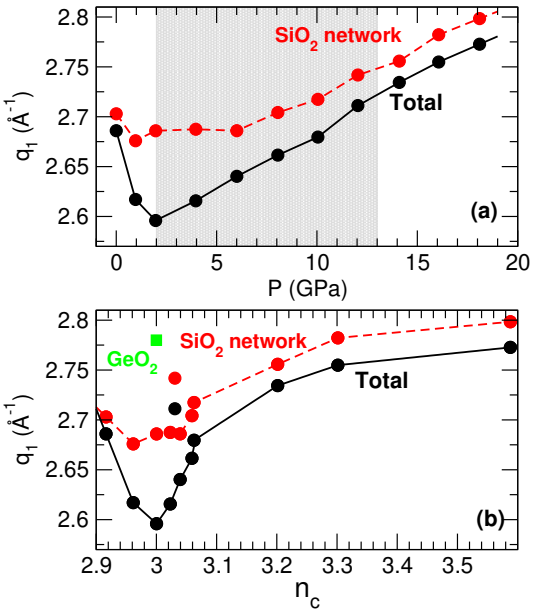

Figure 10. Wave-vector q_1 obtained from the fit of the Bhatia–Thornton pair correlation function $rh_{NN}(r)$ (Fig. 8): (a) $q_1(P)$, (b) $q_1(n_c)$. The gray zone represents the reported reversibility window [37]. Green symbol represent experimental data for GeO_2 [93]. The data point for $GeSe_2$ is out of range (2.10 $Å^{-1}$).

4. Discussion

We relate the anomalies in topological ordering in isostatic systems with a measure of structural disorder, and with diffusivity extrema which underscore water-like anomalies found in densified tetrahedral liquids.

4.1. *Entropy*

An additional and interesting insight is, indeed, provided by the pair correlation entropy which measures from the atom-atom radial distribution functions $g_{ij}(r)$ representing an excess entropy with respect to the entropy of an ideal gas. The latter consists of a non-interacting mixture of particles having the property $g_{ij}(r)$=1 over all distances

$$S_2/k_BN = -2\pi\rho_0 \sum_{i,j} x_i x_j \int_0^\infty \Big[g_{ij}(r) \ln g_{ij}(r) - \big[g_{ij}(r) - 1 \big] \Big] r^2 dr \tag{9}$$

where x_i is the mole fraction of component i and ρ_0 is the number density of the system. The latter quantity permits to capture effects that departs from form random liquid networks and show interesting correlations with calculated thermodynamic and transport extrema occurring in densified tetrahedral liquids, known as "water-like" anomalies. These simply signal deviations from regular liquid behaviour that the excess entropy is able to capture, and are characterized by sets of state points (T,ρ) or (T,P) for which the diffusivity increases with density/pressure.

Figure 11a represents the calculated entropy for the present system, as a function of the constraint density n_c. Unlike the monotonic decrease in S_2 with density ρ as in simple liquids, the present system has a well-defined anomalous regime where the excess entropy rises with increasing density (Figure 11a) or pressure (not shown). The increase of S_2 is large in flexible networks with increasing connectedness, correlated with the increase in density (right axis), and reaches a maximum close at the isostatic condition, while for $n_c \geq 3$ entropy decreases moderately. These are linked with other anomalies noticed in transport coefficients when tracked as a function of P or ρ or n_c [58,80]. Here oxygen diffusivity (and silicon, not represented) displays a minimum D_m at n_c=2.85 and a maximum D_M at $n_c \simeq 3$, whereas Na is merely constant in the flexible phase (Figure 11b), exhibits a dramatic jump in the identified intermediate phase [58] and then decreases in a similar fashion to oxygen in the stressed rigid phase corresponding to the high pressure NS2 system.

A closer inspection of the different Figures 10 and 11 indicates that the structural properties not all track the *locus* of the IP. Parameters characterizing the topological ordering (q_1 and ξ) appear to display a change in behavior as the system is exactly isostatically rigid (n_c=3), i.e. at the flexible to intermediate boundary, whereas structural partial correlations involved in the first sharp diffraction peak merely follow the location of the IP region. On the other hand, previous investigations have shown that the change in dynamic properties (diffusivity) takes place throughout the IP. These features signal that the signatures of the two IP boundaries are essentially detected from calculated dynamic quantities (diffusivity [37, 58], viscosity [80], enthalpy of relaxation [40]) or from experimental thermal/calorimetric measurements [30].

4.2. *Water-like anomalies*

The present behaviors obtained for pair correlation entropy and diffusivity correspond to salient features of water-like anomalies which consist in a series of dynamic/thermodynamic anomalies that manifest by diffusivity maxima and minima in densified tetrahedral liquids such as water [97], SiO_2 [98] or GeO_2 [72,99]. Such anomalies have been found in NS2 as well, and extrema in

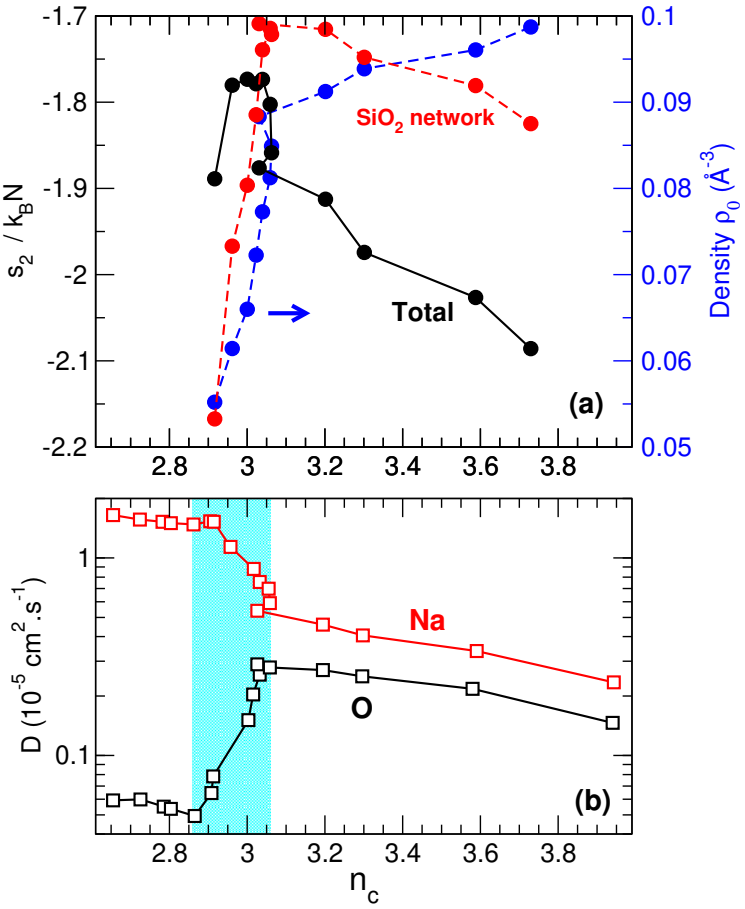

Figure 11. (a) Calculated entropy in densified NS2 (eq. (9) as a function of calculated constraint density n_c. The calculation is performed either on the total network (black) or on the underlying silica network (red). The right axis correspond to the calculated system density (blue symbols). (b) Calculated oxygen and sodium diffusivity as a function of the calculated n_c. Transport properties are obviously affected by the elastic nature of the liquid. Adapted from Bauchy et al. [80] and Mantisi et al. [58]. The location of the reversibility window (cyan) has been determined from NVT cooling-heating cycles [58].

diffusivities with density or pressure for the network forming species (Figure 11b and [58, 69]) or viscosity [80] have been reported. In addition, when both diffusivity and viscosity are studied as a function of temperature in an Arrhenius plot, it has been found that corresponding activation energies for viscosity or diffusion also display a minimum for the same range of pressures/densities where the diffusivity anomalies are found [37]. The latter behavior indicates the increased ease of relaxation in isostatic network-forming liquids that contributes to heterogeneous dynamics [29] and to the nearly reversing character of the glass transition (Figure 3c).

In studies on structural and dynamic anomalies of densified tetrahedral liquids, it has been stressed [97–99] that the definition of local structural order parameters could help in understanding the relationships between such diffusivity anomalies, structural and thermodynamic anomalies under temperature and density change. One order parameter (translational) measures the tendency of pairs of molecules to be separated by a preferential distance, while a second order

parameter (orientational) measures the tendency of a molecule and its nearest neighbours to adopt preferential orientations.

Here, one now recognizes that the isostatic nature of the network leads to structural correlations which manifest by a certain degree of topological ordering characterized by a decay length ξ and a period q_1 that is linked with the presence of an entropy maximum for $n_c \simeq 3$. The diffusivity anomalies are driven by constraint n_c softening which is the dominant feature controling the evolution of transport coefficient under density and temperature change [73]. We, thus, view these transport anomalies as a consequences of structural rearrangements driven by stress adaptation in a connectivity window located between roughly $2.85 \leq n_c \leq 3.0$, and the typical features of diffusivity minima D_m and maxima D_M can be related to the boundaries of the RW (Figure 11b) [37,58]. In light of these correlations, we now interpret the location of D_m as the boundary for the onset of a rigid but stress-free network-forming liquid, whereas the location of D_M is related to the upper boundary of the IP. The trend with n_c (Figure 11b) also reveals that local deformation modes which are present in the flexible phase will promote transport. Once the system is becoming more rigid, atomic motion and diffusivity reduce. In the IP, the adaptive nature of the structure (constraint softening [37,73]) will facilitate transport that is also induced by a reduction of stress [40] (no redundant bonds/constraints), prior to an important decrease once the system has become stressed rigid and the network is locked by an important bond density.

5. Conclusion

Here we have reviewed some features regarding flexible to rigid transitions in glasses and disordered networks. The Phillips–Thorpe mean-field theoretical framework inspired by the Maxwell treatment on trusses has been used for decades in glass science. More recent non-mean-field scenarios indicate that measured reversibility windows at the glass transition might be the signature of the ability of networks to adapt under a stress imposed by composition or pressure, that lead to a so-called intermediate phase. The picture of flexible to rigid transition appears, thus, to be more complex than previously believed, and connects to certain anomalous features typical of densified liquids. Molecular dynamics simulations provide an interesting added value, able to substantiate these key results derived from phenomenological models. Simulated sodium silicates appear as attractive systems in this context given that they undergo a rigidity transition with sodium content, and display with pressure a variety of anomalies that connect to the presence of a reversibility window, and an intermediate phase. Here we have focused essentially on possible structural signatures of the IP, and the analysis of the decay of Bhatia–Thornton pair correlation functions with pressure indicates that typical lengthscales for topological ordering display anomalies (thresholds, minima) across the IP or its related boundaries. These results obtained from number-number correlations might suggest that structural signatures of the IP are only visible from partial correlations, as also previously found in parent systems [60,69].

The NS2 liquid displays striking similarities with densified tetrahedral liquids [97–99] which display similar anomalous thermodynamic and kinetic properties, the most obvious one being the existence of a regime of anomalous density behaviour where diffusivity and entropy maximizes. In contrast to those liquids which do not contain ions (i.e. Na), no negative isothermal expansion coefficient is found that give rise to temperatures of maximum density in appropriate density-temperature or temperature-pressure planes [99]. Instead, one acknowledges an obvious threshold behavior once ρ_0 is tracked with the constraint density n_c (Figure 11b) which only underscores the enhanced compaction tendency of the flexible phase and the rapid evolution of ρ_0 with increasing rigidity.

These anomalies not only correspond to a set of thermodynamic state points for which e.g. the diffusivity increases with density but also underscores the role played by network connectivity

and structure. A unified explanation [100, 101] for such thermodynamic and kinetic anomalies has been proposed on the basis of the existence of an excess entropy anomaly involving a rise in excess entropy on isothermal compression. The collection of numerical data on NS2, once represented as a function of constraint density n_c highlights now the central role of network rigidity and provides some indication that stretching and bending interaction softening [37, 73] will control the various obtained anomalies including the one detected in pair correlation entropy, while also driving the onset of a near reversible glass transition where the enthalpy of relaxation is minimal. This is the dominant feature of the intermediate phase. Ultimately, these features give rise to some structural ordering that manifests once long-range correlations of the network topology are investigated as a function of the order parameter of the flexible to rigid transition, i.e. the fraction of floppy modes 3-n_c.

Conflicts of interest

The author has no conflict of interest to declare.

References

[1] E. Bychkov, C. J. Benmore, D. L. Price, "Compositional changes of the first sharp diffraction peak in binary selenide glasses", *Phys. Rev. B* **72** (2005), no. 17, article no. 172107.

[2] S. Salmon, R. A. Martin, P. E. Mason, G. J. Cuello, "Topological versus chemical ordering in network glasses at intermediate and extended length scales", *Nature* **435** (2005), p. 75-78.

[3] P. S. Salmon, A. C. Barnes, R. A. Martin, G. J. Cuello, "Structure of glassy GeO_2", *J. Phys.: Condens. Matter* **19** (2007), no. 41, article no. 415110.

[4] F. L. Galeener, G. Lucovsky, "Longitudinal Optical Vibrations in Glasses: GeO_2 and SiO_2", *Phys. Rev. Lett.* **37** (1976), no. 22, p. 1474-1478.

[5] G. Ferlat, T. Charpentier, A. P. Seitsonen, A. Takada, M. Lazzeri, L. Cormier, G. Calas, F. Mauri, "Boroxol Rings in Liquid and Vitreous B_2O_3 from First Principles", *Phys. Rev. Lett.* **101** (2008), no. 6, article no. 065504.

[6] K. Vignarooban, P. Boolchand, M. Micoulaut, M. Malki, W. J. Bresser, "Rigidity transitions in glasses driven by changes in network dimensionality and structural groupings", *Eur. Phys. Lett.* **108** (2014), no. 5, article no. 56001.

[7] H. Liu, Z. Zhao, Q. Zhou, R. Chen, K. Yang, Z. Wang, L. Tang, M. Bauchy, "Challenges and opportunities in atomistic simulations of glasses: a review", *Comptes Rendus. Géoscience* (2022), Online first.

[8] J. C. Maxwell, "L. *On* the calculation of the equilibrium and stiffness of frames", *The London, Edinburgh, and Dublin Philosophical Magazine and Journal of Science* **27** (1864), no. 182, p. 294-299.

[9] J. C. Phillips, "Topology of covalent non-crystalline solids I: Short-range order in chalcogenide alloys", *J. Non Cryst. Solids* **34** (1979), no. 2, p. 153-181.

[10] M. F. Thorpe, "Continuous deformations in random networks", *J. Non Cryst. Solids* **57** (1983), no. 3, p. 355-370.

[11] P. Boolchand, M. F. Thorpe, "Glass-forming tendency, percolation of rigidity, and onefold-coordinated atoms in covalent networks", *Phys. Rev. B* **50** (1994), no. 14, p. 10366-10368.

[12] M. Zhang, P. Boolchand, "The Central Role of Broken Bond-Bending Constraints in Promoting Glass Formation in the Oxides", *Science* **266** (1994), no. 5189, p. 1355-1357.

[13] M. Micoulaut, "Amorphous materials: Properties, structure, and durability: Constrained interactions, rigidity, adaptative networks, and their role for the description of silicates", *Am. Mineral.* **93** (2008), no. 11-12, p. 1732-1748.

[14] M. Micoulaut, H. Flores-Ruiz, "Search for a possible flexible-to-rigid transition in models of phase change materials", *Phys. Rev. B* **103** (2021), no. 13, article no. 134206.

[15] M. F. Thorpe, D. J. Jacobs, M. V. Chubynsky, J. C. Phillips, "Self-organization in network glasses", *J. Non Cryst. Solids* **266-269** (2000), p. 859-866.

[16] H. He, M. F. Thorpe, "Elastic Properties of Glasses", *Phys. Rev. Lett.* **54** (1985), no. 19, p. 2107-2110.

[17] W. A. Kamitakahara, R. L. Cappelletti, P. Boolchand, B. L. Halfpap, F. Gompf, D. A. Neumann, H. Mutka, "Vibrational densities of states and network rigidity in chalcogenide glasses", *Phys. Rev. B* **44** (1991), no. 1, p. 94-100.

[18] X. Feng, W. J. Bresser, P. Boolchand, "Direct Evidence for Stiffness Threshold in Chalcogenide Glasses", *Phys. Rev. Lett.* **78** (1997), no. 23, p. 4422-4425.

[19] R. Böhmer, C. A. Angell, "Correlations of the nonexponentiality and state dependence of mechanical relaxations with bond connectivity in Ge-As-Se supercooled liquids", *Phys. Rev. B* **45** (1992), no. 17, p. 10091-10094.

[20] M. Tatsumisago, B. L. Halfpap, J. L. Green, S. M. Lindsay, C. A. Angell, "Fragility of Ge-As-Se glass-forming liquids in relation to rigidity percolation, and the Kauzmann paradox", *Phys. Rev. Lett.* **64** (1990), no. 13, p. 1549-1552.
[21] K. Gunasekera, S. Bhosle, P. Boolchand, M. Micoulaut, "Superstrong nature of covalently bonded glass-forming liquids at select compositions", *J. Chem. Phys.* **139** (2013), no. 16, article no. 164511.
[22] S. Ravindren, K. Gunasekera, Z. Tucker, A. Diebold, P. Boolchand, M. Micoulaut, "Crucial effect of melt homogenization on the fragility of non-stoichiometric chalcogenides", *J. Chem. Phys.* **140** (2014), no. 13, article no. 134501.
[23] Y. Vaills, T. Qu, M. Micoulaut, F. Chaimbault, P. Boolchand, "Direct evidence of rigidity loss and self-organization in silicate glasses", *J. Phys.: Condens. Matter* **17** (2005), no. 32, p. 4889-4896.
[24] D. I. Novita, P. Boolchand, M. Malki, M. Micoulaut, "Fast-Ion Conduction and Flexibility of Glassy Networks", *Phys. Rev. Lett.* **98** (2007), no. 19, article no. 195501.
[25] M. Micoulaut, M. Malki, "Direct Evidence of a Characteristic Length Scale of a Dynamical Nature in the Boolchand Phase of Glasses", *Phys. Rev. Lett.* **105** (2010), no. 23, article no. 235504.
[26] M. Micoulaut, M. Malki, D. I. Novita, P. Boolchand, "Fast-ion conduction and flexibility and rigidity of solid electrolyte glasses", *Phys. Rev. B* **80** (2009), no. 18, p. 184205.
[27] L. Yan, M. Wyart, "Evolution of Covalent Networks under Cooling: Contrasting the Rigidity Window and Jamming Scenarios", *Phys. Rev. Lett.* **113** (2014), no. 21, article no. 215504.
[28] M. Bauchy, M. Micoulaut, "Percolative heterogeneous topological constraints and fragility in glass-forming liquids", *Eur. Phys. Lett.* **104** (2013), no. 5, article no. 56002.
[29] M. Micoulaut, M. Bauchy, "Evidence for Anomalous Dynamic Heterogeneities in Isostatic Supercooled Liquids", *Phys. Rev. Lett.* **118** (2017), no. 14, article no. 145502.
[30] M. Micoulaut, "Concepts and applications of rigidity in non-crystalline solids: a review on new developments and directions", *ADV PHYS-X* **1** (2016), no. 2, p. 147-175.
[31] J. Barré, A. R. Bishop, T. Lookman, A. Saxena, "Adaptability and "Intermediate Phase" in Randomly Connected Networks", *Phys. Rev. Lett.* **94** (2005), no. 20, article no. 208701.
[32] M. Micoulaut, J. C. Phillips, "Rings and rigidity transitions in network glasses", *Phys. Rev. B* **67** (2003), no. 10, article no. 104204.
[33] M. Micoulaut, "Rigidity and intermediate phases in glasses driven by speciation", *Phys. Rev. B* **74** (2006), no. 18, article no. 184208.
[34] M.-A. Brière, M. V. Chubynsky, N. Mousseau, "Self-organized criticality in the intermediate phase of rigidity percolation", *Phys. Rev. E* **75** (2007), no. 5, article no. 056108.
[35] L. Yan, "Entropy favors heterogeneous structures of networks near the rigidity threshold", *Nat. Commun.* **9** (2018), no. 1, article no. 1359.
[36] C. F. Moukarzel, "Two rigidity-percolation transitions on binary Bethe networks and the intermediate phase in glass", *Phys. Rev. E* **88** (2013), no. 6, article no. 062121.
[37] M. Bauchy, M. Micoulaut, "Densified network glasses and liquids with thermodynamically reversible and structurally adaptive behaviour", *Nat. Commun.* **6** (2015), no. 1, p. 6398.
[38] F. Wang, S. Mamedov, P. Boolchand, B. Goodman, M. Chandrasekhar, "Pressure Raman effects and internal stress in network glasses", *Phys. Rev. B* **71** (2005), no. 17, article no. 174201.
[39] S. Bhosle, K. Gunasekera, P. Boolchand, M. Micoulaut, "Melt Homogenization and Self-Organization in Chalcogenides-Part II", *Int. J. Appl. Glass Sci.* **3** (2012), no. 3, p. 205-220.
[40] W. Song, X. Li, M. Wang, M. Bauchy, M. Micoulaut, "Dynamic and stress signatures of the rigid intermediate phase in glass-forming liquids", *J. Chem. Phys.* **152** (2020), no. 22, article no. 221101.
[41] G. Sreevidya Varma, C. Das, S. Asokan, "Evidence of an intermediate phase in a quaternary Ag bearing telluride glass system using alternating DSC", *Solid State Commun.* **177** (2014), p. 108-112.
[42] D. Selvanathan, W. J. Bresser, P. Boolchand, "Stiffness transitions in Si_xSe_{1-x} glasses from Raman scattering and temperature-modulated differential scanning calorimetry", *Phys. Rev. B* **61** (2000), no. 22, p. 15061-15076.
[43] S. Chakraborty, P. Poolchand, "Topological origin of fragility, network adaptation, and rigidity and stress transitions in especially homogenized nonstoichiometric binary Ge_xS_{100-x} glasses", *J. Phys. Chem. B* **118** (2014), no. 8, p. 2249-2263.
[44] C. Mohanty, A. Mandal, V. K. Gogi, P. Chen, D. I. Novita, R. Chbeir, M. Bauchy, M. Micoulaut, P. Boolchand, "Linking Melt Dynamics With Topological Phases and Molecular Structure of Sodium Phosphate Glasses From Calorimetry, Raman Scattering, and Infrared Reflectance", *Front. Mater.* **6** (2019).
[45] K. Rompicharla, D. I. Novita, P. Chen, P. Boolchand, M. Micoulaut, W. Huff, "Abrupt boundaries of intermediate phases and space filling in oxide glasses", *J. Phys.: Condens. Matter* **20** (2008), no. 20, article no. 202101.
[46] C. Das, M. S. R. N. Kiran, U. Ramamurty, S. Asokan, "Manifestation of intermediate phase in mechanical properties: Nano-indentation studies on Ge-Te-Si bulk chalcogenide glasses", *Solid State Commun.* **152** (2012), no. 24, p. 2181-2184.
[47] K. Gunasekera, P. Boolchand, M. Micoulaut, "Effect of mixed Ge/Si cross-linking on the physical properties of amorphous Ge-Si-Te networks", *J. Appl. Phys.* **115** (2014), no. 16, article no. 164905.

[48] K. Gunasekera, P. Boolchand, M. Micoulaut, "Elastic Phases of $Ge_xSb_xSe_{100-2x}$ Ternary Glasses Driven by Topology", *J. Phys. Chem. B* **117** (2013), no. 34, p. 10027-10034.

[49] U. Vempati, P. Boolchand, "The thermally reversing window in ternary $Ge_xAs_xS_{1-2x}$ glasses", *J. Phys.: Condens. Matter* **16** (2004), no. 44, p. S5121-S5138.

[50] S. Chakravarty, D. G. Georgiev, P. Boolchand, M. Micoulaut, "Ageing, fragility and the reversibility window in bulk alloy glasses", *J. Phys.: Condens. Matter* **17** (2004), no. 1, p. L1-L7.

[51] T. Qu, P. Boolchand, "Shift in elastic phase boundaries due to nanoscale phase separation in network glasses: the case of $Ge_xAs_xS_{1-2x}$", *Philos. Mag.* **85** (2005), no. 8, p. 875-884.

[52] R. Chbeir, M. Bauchy, M. Micoulaut, P. Boolchand, "Evidence for a Correlation of Melt Fragility Index With Topological Phases of Multicomponent Glasses", *Front. Mater.* **6** (2019).

[53] Y. Wang, J. Wells, D. G. Georgiev, P. Boolchand, K. A. Jackson, M. Micoulaut, "Sharp Rigid to Floppy Phase Transition Induced by Dangling Ends in a Network Glass", *Phys. Rev. Lett.* **87** (2001), no. 18, article no. 185503.

[54] F. Wang, P. Boolchand, K. A. Jackson, M. Micoulaut, "Chemical alloying and light-induced collapse of intermediate phases in chalcohalide glasses", *J. Phys.: Condens. Matter* **19** (2007), no. 22, article no. 226201.

[55] P. Boolchand, P. Chen, U. Vempati, "Intermediate Phases, structural variance and network demixing in chalcogenides: The unusual case of group V sulfides", *J. Non Cryst. Solids* **355** (2009), no. 37-42, p. 1773-1785, Non-Oxide and New Optical Glasses 16.

[56] D. G. Georgiev, P. Boolchand, H. Eckert, M. Micoulaut, K. A. Jackson, "The self-organized phase of bulk P_xSe_{1-x} glasses", *Eur. Phys. Lett.* **62** (2003), no. 1, p. 49-55.

[57] S. Chakravarty, R. Chbeir, P. Chen, M. Micoulaut, P. Boolchand, "Correlating Melt Dynamics and Configurational Entropy Change With Topological Phases of As_xS100_{100-x} Glasses and the Crucial Role of Melt/Glass Homogenization", *Front. Mater.* **6** (2019).

[58] B. Mantisi, M. Bauchy, M. Micoulaut, "Cycling through the glass transition: Evidence for reversibility windows and dynamic anomalies", *Phys. Rev. B* **92** (2015), no. 13, article no. 134201.

[59] K. Trachenko, M. T. Dove, V. Brazhkin, F. S. El'kin, "Network Rigidity and Properties of SiO_2 and GeO_2 Glasses under Pressure", *Phys. Rev. Lett.* **93** (2004), no. 13, article no. 135502.

[60] M. Micoulaut, M. Bauchy, "Anomalies of the first sharp diffraction peak in network glasses: Evidence for correlations with dynamic and rigidity properties", *Phys. Status Solidi B Basic Res.* **250** (2013), no. 5, p. 976-982.

[61] Y. Wang, E. Ohata, S. Hosokawa, M. Sakurai, E. Matsubara, "Intermediate-range order in glassy Ge_xSe_{1-x} around the stiffness transition composition", *J. Non Cryst. Solids* **337** (2004), no. 1, p. 54-61.

[62] D. Sharma, S. Sampath, N. P. Lalla, A. M. Awasthi, "Mesoscopic organization and structural phases in network-forming Ge_xSe_{1-x} glasses", *Physica B Condens. Matter* **357** (2005), no. 3, p. 290-298.

[63] M. T. Shatnawi, C. L. Farrow, P. Chen, P. Boolchand, A. Sartbaeva, M. F. Thorpe, S. J. L. Billinge, "Search for a structural response to the intermediate phase in Ge_xSe_{1-x} glasses", *Phys. Rev. B* **77** (2008), no. 9, article no. 094134.

[64] P. Lucas, E. A. King, O. Gulbiten, J. L. Yarger, E. Soignard, B. Bureau, "Bimodal phase percolation model for the structure of Ge-Se glasses and the existence of the intermediate phase", *Phys. Rev. B* **80** (2009), no. 21, article no. 214114.

[65] E. L. Gjersing, S. Sen, B. G. Aitken, "Structure, Connectivity, and Configurational Entropy of Ge_xSe_{100-x} Glasses: Results from ^{77}Se MAS NMR Spectroscopy", *J. Phys. Chem. C* **114** (2010), no. 18, p. 8601-8608.

[66] G. Chen, F. Inam, D. A. Drabold, "Structural origin of the intermediate phase in Ge–Se glasses", *Appl. Phys. Lett.* **97** (2010), no. 13, article no. 131901.

[67] A. Zeidler, P. S. Salmon, D. A. J. Whittaker, K. J. Pizzey, A. C. Hannon, "Topological Ordering and Viscosity in the Glass-Forming Ge-Se System: The Search for a Structural or Dynamical Signature of the Intermediate Phase", *Front. Mater.* **4** (2017).

[68] F. Inam, M. T. Shatnawi, D. Tafen, S. J. L. Billinge, P. Chen, D. A. Drabold, "An intermediate phase in Ge_xSe_{1-x} glasses: experiment and simulation", *J. Phys.: Condens. Matter* **19** (2007), no. 45, article no. 455206.

[69] M. Bauchy, M. Micoulaut, M. Boero, C. Massobrio, "Compositional Thresholds and Anomalies in Connection with Stiffness Transitions in Network Glasses", *Phys. Rev. Lett.* **110** (2013), no. 16, article no. 165501.

[70] M. Bauchy, A. Kachmar, M. Micoulaut, "Structural, dynamic, electronic, and vibrational properties of flexible, intermediate, and stressed rigid As-Se glasses and liquids from first principles molecular dynamics", *J. Chem. Phys.* **141** (2014), no. 19, article no. 194506.

[71] S. Chakraborty, P. Boolchand, M. Micoulaut, "Structural properties of Ge-S amorphous networks in relationship with rigidity transitions: An *ab initio* molecular dynamics study", *Phys. Rev. B* **96** (2017), no. 9, article no. 094205.

[72] F. Pacaud, M. Micoulaut, "Thermodynamic precursors, liquid-liquid transitions, dynamic and topological anomalies in densified liquid germania", *J. Chem. Phys.* **143** (2015), no. 6, article no. 064502.

[73] M. Bauchy, M. Micoulaut, "Transport Anomalies and Adaptative Pressure-Dependent Topological Constraints in Tetrahedral Liquids: Evidence for a Reversibility Window Analogue", *Phys. Rev. Lett.* **110** (2013), no. 9, article no. 095501.

[74] M. Wilson, "Model investigations of network-forming materials", *Phys. Chem. Chem. Phys.* **14** (2012), no. 37, p. 12701-12714.
[75] A. N. Cormack, J. Du, T. R. Zeitler, "Sodium ion migration mechanisms in silicate glasses probed by molecular dynamics simulations", *J. Non Cryst. Solids* **323** (2003), no. 1, p. 147-154.
[76] J. Du, A. N. Cormack, "The medium range structure of sodium silicate glasses: a molecular dynamics simulation", *J. Non Cryst. Solids* **349** (2004), p. 66-79, Glass Science for High Technology. 16th University Conference on Glass Science.
[77] N. M. Anoop Krishnan, R. Ravinder, R. Kumar, Y. Le Pape, G. Sant, M. Bauchy, "Density-stiffness scaling in minerals upon disordering: Irradiation vs. vitrification", *Acta Mater.* **166** (2019), p. 611-617.
[78] M. Bauchy, "Structural, vibrational, and elastic properties of a calcium aluminosilicate glass from molecular dynamics simulations: The role of the potential", *J. Chem. Phys.* **141** (2014), no. 2, article no. 024507.
[79] J. Du, L. René Corrales, "Compositional dependence of the first sharp diffraction peaks in alkali silicate glasses: A molecular dynamics study", *J. Non Cryst. Solids* **352** (2006), no. 30, p. 3255-3269.
[80] M. Bauchy, B. Guillot, M. Micoulaut, N. Sator, "Viscosity and viscosity anomalies of model silicates and magmas: A numerical investigation", *Chem. Geol.* **346** (2013), p. 47-56, 9$^{\text{th}}$ Silicate Melts Workshop.
[81] G. J. Kramer, A. J. M. De Man, R. A. Van Santen, "Zeolites versus aluminosilicate clusters: the validity of a local description", *J. Am. Chem. Soc.* **113** (1991), no. 17, p. 6435-6441.
[82] M. Bauchy, M. Micoulaut, "Atomic scale foundation of temperature-dependent bonding constraints in network glasses and liquids", *J. Non Cryst. Solids* **357** (2011), no. 14, p. 2530-2537.
[83] M. Micoulaut, A. Kachmar, M. Bauchy, S. Le Roux, C. Massobrio, M. Boero, "Structure, topology, rings, and vibrational and electronic properties of Ge_xSe_{1-x} glasses across the rigidity transition: A numerical study", *Phys. Rev. B* **88** (2013), no. 5, article no. 054203.
[84] C. Yildirim, J.-Y. Raty, M. Micoulaut, "Revealing the role of molecular rigidity on the fragility evolution of glass-forming liquids", *Nat. Commun.* **7** (2016), article no. 11086.
[85] A. B. Bhatia, D. E. Thornton, "Structural Aspects of the Electrical Resistivity of Binary Alloys", *Phys. Rev. B* **2** (1970), no. 8, p. 3004-3012.
[86] B. Grosdidier, "Two conceptualizations of the partial structures and of the order parameters in the ternary alloy and relationships between them", *J. Non Cryst. Solids* **566** (2021), article no. 120894.
[87] R. Evans, R. J. F. Leote de Carvalho, J. R. Henderson, D. C. Hoyle, "Asymptotic decay of correlations in liquids and their mixtures", *J. Chem. Phys.* **100** (1994), no. 1, p. 591-603.
[88] D. Ma, A. Stoica, X. L. Wang, "Power-law scaling and fractal nature of medium-range order in metallic glasses", *Nature Mater.* **8** (2009), p. 30-34.
[89] T. Freltoft, J. K. Kjems, S. K. Sinha, "Power-law correlations and finite-size effects in silica particle aggregates studied by small-angle neutron scattering", *Phys. Rev. B* **33** (1986), no. 1, p. 269-275.
[90] J.-P. Hansen, R. Mac Donald, *Theory of Simple Liquids*, Cambridge University Press, 1976.
[91] P. S. Salmon, A. Zeidler, "Identifying and characterising the different structural length scales in liquids and glasses: an experimental approach", *Phys. Chem. Chem. Phys.* **15** (2013), no. 37, p. 15286-15308.
[92] R. J. F. Leote de Carvalho, R. Evans, "The decay of correlations in ionic fluids", *Mol. Phys.* **83** (1994), no. 4, p. 619-654.
[93] P. S. Salmon, "Decay of the pair correlations and small-angle scattering for binary liquids and glasses", *J. Phys.: Condens. Matter* **18** (2006), no. 2, article no. 11443.
[94] R. Kjellander, B. Forsberg, "Ionic fluids with r^{-6} pair interactions have power-law electrostatic screening", *J. Phys. A, Math. Gen.* **38** (2005), no. 24, p. 5405-5424.
[95] C. Grodon, M. Dijkstra, R. Evans, R. Roth, "Homogeneous and inhomogeneous hard-sphere mixtures: manifestations of structural crossover", *Mol. Phys.* **103** (2005), no. 21-23, p. 3009-3023.
[96] M. Bauchy, M. Micoulaut, M. Celino, S. Le Roux, M. Boero, C. Massobrio, "Angular rigidity in tetrahedral network glasses with changing composition", *Phys. Rev. B* **84** (2011), no. 5, article no. 054201.
[97] J. R. Errington, P. G. Debenedetti, "Relationship between structural order and the anomalies of liquid water", *Nature* **409** (2001), p. 318-321.
[98] M. S. Shell, P. G. Debenedetti, A. Z. Panagiotopoulos, "Molecular structural order and anomalies in liquid silica", *Phys. Rev. E* **66** (2002), no. 1, article no. 011202.
[99] B. S. Jabes, M. Agarwal, C. Chakravarty, "Tetrahedral order, pair correlation entropy, and waterlike liquid state anomalies: Comparison of GeO_2 with BeF_2, SiO_2, and H_2O", *J. Chem. Phys.* **132** (2010), no. 23, article no. 234507.
[100] R. Sharma, S. N. Chakraborty, C. Chakravarty, "Entropy, diffusivity, and structural order in liquids with waterlike anomalies", *J. Chem. Phys.* **125** (2006), no. 20, article no. 204501.
[101] M. Agarwal, R. Sharma, C. Chakravarty, "Ionic melts with waterlike anomalies: Thermodynamic properties of liquid BeF2", *J. Chem. Phys.* **127** (2007), no. 16, article no. 164502.